

Star Formation in a Cosmological Simulation of Reionization

A. Gayler Harford¹ and Nickolay Y. Gnedin^{2,3,4}

ABSTRACT

We study the luminosity functions of high-redshift galaxies in detailed hydrodynamic simulations of cosmic reionization, which are designed to reproduce the evolution of the Lyman- α forest between $z \sim 5$ and $z \sim 6$. We find that the luminosity functions and total stellar mass densities are in agreement with observations when plausible assumptions about reddening at $z \sim 6$ are made. Our simulations support the conclusion that stars alone reionized the universe.

Subject headings: cosmology: theory - cosmology: large-scale structure of universe - galaxies: evolution - galaxies: formation - galaxies: high-redshift - galaxies: starburst - galaxies: stellar content - infrared: galaxies

1. Introduction

An important issue in cosmology today is the timing and mechanism of the reionization of the universe. Since the early work of Madau et al. (1999), stars have been thought to be prime candidates for the energy source, since the Gunn-Peterson trough disappears prior to the presumed epoch of quasars ($z > 5$).

However, compounding the problem of identifying the primary sources of cosmic reionization are recent HST observations of galaxies at $z \sim 6$ (Bouwens et al. 2004; Bunker et al. 2004; Yan & Windhorst 2004; Giavalisco et al. 2004; Hu et al. 2005; Bouwens et al. 2006). It remains controversial whether enough stellar luminosity has actually been observed to account for reionization at $z \sim 6$, as is seen in the spectra of SDSS quasars (White et al. 2003; Fan et al. 2006).

On the other hand, both numerical simulations (Gnedin 2000; Harford & Gnedin 2003; Springel & Hernquist 2003; Gnedin 2004) and

semi-analytical models (Night et al. 2006) predict star formation rates at $z \sim 6$ nearly as large as those at $z \sim 4$, in direct conflict with some of the observational studies (Bunker et al. 2004), but in agreement with recent studies of Lyman- α emitting galaxies at $z \sim 6$ (Hu et al. 2005), which suggest that the star formation rate at $z \sim 6$ is substantially higher than that found by HST observations.

While the observational determination of the star formation rate at $z \sim 6$ will most likely remain controversial for some time, in this paper we focus on a theoretical aspect of this problem. Of course, predicting *a priori* the absolute value of the average star formation rate in the universe at $z \sim 6$ is not possible with our current understanding of the galaxy formation process, in large part because the efficiency of star formation in molecular clouds at high redshift is not known. However, modern cosmological simulations are sufficiently robust to predict the *ratio* of star formation rates at, say, $z \sim 4$ and $z \sim 6$. Thus, we can legitimately attempt to answer the following question:

After imposing a requirement on a theoretical model to reproduce the observed evolution of the Lyman- α forest between $z = 4$ and $z = 6$, would it be possible, by appropriately adjusting the star formation efficiency as a free parameter, to fit simultaneously galaxy luminosity functions at $z \approx 4$ and $z \approx 6$?

¹JILA, University of Colorado and National Institute of Standards and Technology, Boulder, CO 80309, USA; gharford@sif.colorado.edu

²Particle Astrophysics Center, Fermi National Accelerator Laboratory, Batavia, IL 60510, USA; gnedin@fnal.gov

³Department of Astronomy & Astrophysics, The University of Chicago, Chicago, IL 60637, USA

⁴Kavli Institute for Cosmological Physics, The University of Chicago, Chicago, IL 60637, USA

In addition, we can use the recent observational estimates of the total stellar mass density at $z \approx 5$ as an extra constraint.

In this paper we use cosmological simulations of reionization as our theoretical model. The main advantage of our set of simulations is that they are not only able to resolve high redshift galaxies, but, by virtue of including radiative transfer of ionizing radiation, are also able to reproduce the mean properties of the observed Lyman- α forest between redshifts 5 and 6 (Gnedin & Fan 2006). In particular, our simulations are consistent with the end of the reionization at $z \approx 6$, clearly seen in the SDSS data (Fan et al. 2006).

Thus, we attempt to place both the observations of the Lyman- α forest at $z > 5$ and the observations of star-forming galaxies at the same cosmic epoch into a unified picture, in which the same simulation is required to fit *all* available observational data.

We briefly describe the simulations in §2, present the star formation rates in §3.1, discuss numerical resolution issues in §3.2, present our luminosity functions in §3.3, and discuss the accumulation of stellar mass in §3.4. In §4 we conclude and discuss the results.

2. Method

Simulations used in this paper have been run with the “Softened Lagrangian Hydrodynamics” (SLH) code Gnedin (2000, 2004). The simulations include dark matter, gas, star formation, chemistry, and ionization balance in the primordial plasma, and three-dimensional radiative transfer. A flat Λ CDM cosmology with values of cosmological parameters as determined by the first year WMAP data (Spergel et al. 2003) is used throughout this paper.

The radiative transfer is modeled using the Optically Thin Variable Eddington Tensor (OTVET) method of Gnedin & Abel (2001). While OTVET is an approximation, its main advantage is that it is self-consistently coupled to the rest of the simulation code, and thus takes into account possible feedbacks among star formation, radiative transfer, and gas dynamics on spatial and temporal scales resolved in a simulation.

Star formation is incorporated in the simulations using a phenomenological Schmidt law on

scales below the resolution limit of the simulation (i.e. stars are allowed to form wherever the gas sinks below the resolution limit, irrespective of the large-scale environment or mass of the dark matter halo they are forming within). This law introduces a free parameter: the star formation efficiency ϵ_{SF} [as defined by eq. (1) of Gnedin (2000)]. In order to incorporate the uncertainty in this parameter in our results, we use three different simulations in this paper. All of them have a simulation volume of $8h^{-1}$ comoving Mpc. The first two simulations include 128^3 dark matter particles and the same number of quasi-Lagrangian mesh cells for the gas evolution. The third simulation includes 8 times more (256^3) resolution elements in the same simulation volume.

There are two adjustable parameters in our simulations: the efficiency of star formation ϵ_{SF} and the ionizing efficiency, i.e. the amount of ionizing radiation emitted per unit mass of stars. This latter value depends upon the fraction of ionizing photons escaping from the vicinity of a star forming region to the spatial scales resolved in the simulation, a value that is unknown and possibly variable. Our simulations make no assumptions about the value of the ionizing efficiency¹; rather the ionizing efficiency is adjusted to fit the observational data on the Gunn-Peterson absorption in the spectra of SDSS quasars, as explained in Gnedin & Fan (2006).

The ionization history of the universe depends almost completely upon a product of the star formation efficiency and the ionizing efficiency, i.e. the factor that determines how many ionizing photons are emitted per unit mass of dense and rapidly cooling gas (which is assumed to be transforming into stars). For each run the ionizing efficiency is selected so that the simulation is consistent with the observed evolution of the mean transmitted flux in the Lyman- α forest at $z \sim 6$ (White et al. 2003; Songaila 2004; Fan et al. 2006). The star formation efficiency is then treated as the sole free parameter.

¹Note that the ionizing efficiency parameter is related to the fraction of photons escaped from the resolution limit of a simulation. It is *not* directly related to the escape fraction from the virial radius, a quantity often used in analytical models. Computing the escape fraction from the virial radius is a formidable computational task, requiring much higher resolution simulations that we use here.

Table 1: Simulation Parameters

Run	Δx^a	ΔM^b	ϵ_{SF}^c	z_f^d
LowResHighSFR	2	2.6×10^7	0.15	4
LowResLowSFR	2	2.6×10^7	0.05	4
HighResLowSFR	0.64	3.2×10^6	0.05	5.1

^aSpatial resolution in h^{-1} kpc.

^bMass resolution in M_{\odot} .

^cStar formation efficiency.

^dFinal redshift of simulation.

The parameters of the three simulations are listed in Table 1. The two smaller boxes (we label them “LowRes”) are identical, except for the value of the star formation efficiency, which is different by a factor of 3 between the two simulations. The larger simulation (“HighRes”) has the same star formation efficiency as the second LowRes simulation. To make the referral to a specific simulation clear, we use the names that reflect the resolution and star formation efficiencies of our simulations.

Galaxies in the simulation are associated with gravitationally bound objects, identified with the DENMAX algorithm (Bertschinger & Gelb 1991).

Population synthesis is carried out using the STARBURST99 package (Leitherer et al. 1999) with the high mass loss Geneva tracks as described previously (Harford & Gnedin 2003) using a metallicity of 0.001 (0.05 solar) and a galaxy escape fraction for ionizing photons of 0.1. The results were adjusted to reflect a three exponent initial mass function, the “canonical” function given in Weidner & Kroupa (2006). Also included is the emission of extra Lyman- α photons due to the recombination of ionized hydrogen. Throughout the paper AB magnitudes (Oke & Gunn 1983) are used exclusively.

Reddening was computed according to Calzetti (1997). A color excess of 0.15 was included for $z \approx 4$ galaxies (Shapley et al. 2001). For galaxies at $z \approx 6$ we present results both without reddening (Stanway et al. 2005) and with a color excess of 0.05 (Bouwens et al. 2006). For the luminosity functions in Figure 6 unreddened luminosities were multiplied by a factor of 1.8 to make them comparable to reddening with a color excess of 0.05.

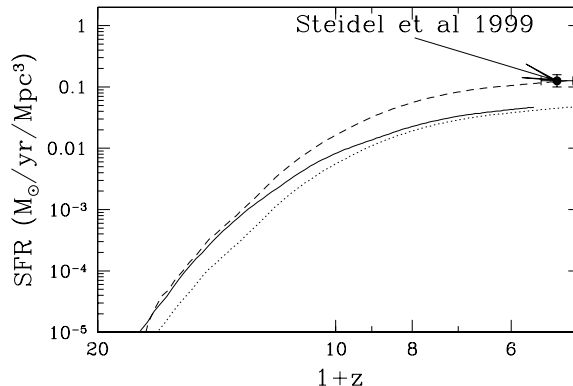


Fig. 1.— Star formation rate as a function of redshift for our three simulations: HighResLowSFR (solid line), LowResLowSFR (dotted line), and LowResHighSFR (dashed line). The filled open circle shows the estimate of the average star formation rate at $z = 4$ from Steidel et al. (1999).

3. Results

3.1. Star Formation Rate in the Simulations

Figure 1 shows the evolution of the star formation history in the three simulations described above. As we emphasized above, all three runs are adjusted to reproduce the observed evolution of the mean transmitted flux in the Lyman- α transition of neutral hydrogen above $z \approx 5$ reasonably well, so the reionization histories are very similar in all three simulations and are consistent with the existing data. The star formation histories in the three runs are, however, quite different. The two low resolution simulations differ by approximately a factor of 3 by construction, since the star formation efficiency is different by that factor between them. The high resolution simulation has the same star formation efficiency as the LowResLowSFR run, but forms more stars at earlier times due to higher spatial resolution. In all simulations the star formation rate begins to flatten significantly at $z \lesssim 7$.

We have examined in detail two snapshots in time: $z = 4$ (1.5 Gyr after the Big Bang), the latest time of the low resolution simulations, and $z = 5.8$ (0.99 Gyr after the Big Bang). Hereafter, unless specified otherwise, we use our HighResLowSFR simulation as a fiducial model for the

$z = 5.8$ snapshot, and the LowResLowSFR simulation as a fiducial model for the $z = 4$ snapshot; the HighResLowSFR simulation was not continued until $z = 4$ due to computational expense.

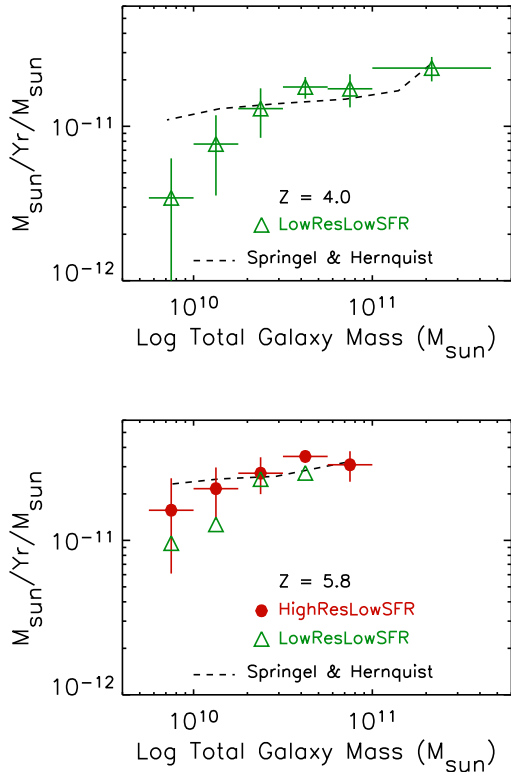


Fig. 2.— Specific star formation rate (SFR per galaxy mass) vs the total galaxy mass for simulated galaxies at $z = 4$ (top panel) and at $z = 5.8$ (bottom panel). The horizontal lines represent galaxy mass ranges, and the vertical lines are standard deviations. The lines are omitted for the LowResLSFR case in the bottom panel for clarity. The dashed lines are the results of Springel & Hernquist (2003).

Deducing the global star formation rate by observing individual galaxies requires knowledge of how star formation is distributed among galaxies of different magnitudes. In order to test the robustness of the simulations in predicting this dependence theoretically, we compare our star formation rates in galaxies of various masses with the simulations by Springel & Hernquist (2003), who conducted extensive resolution and

numerical convergence studies. The results of this comparison are shown in Figure 2. As one can see, the LowResLowSFR run underestimates specific star formation rates in galaxies with $M \lesssim 2 \times 10^{10} M_{\odot}$ at both redshifts, while the HighResLowSFR is consistent with the results of Springel & Hernquist (2003).

It is important to underscore that the physics of gas cooling included in our and Springel & Hernquist (2003) simulations is rather different: while Springel & Hernquist (2003) only include equilibrium cooling of primeval (i.e. metal-free) plasma, in our simulations non-equilibrium radiative transfer effects are taken into account. In addition, we include cooling from heavy elements and molecular hydrogen. It is therefore somewhat unexpected that the two sets of simulations agree so well. On the other hand, if this agreement is not a mere coincidence, it emphasizes the robustness of modern cosmological simulations in predicting total rates of star formation in well resolved galaxies (within the adopted phenomenological recipe of star formation, of course).

It is interesting to note that for the same mass the higher redshift galaxies have a somewhat greater star formation rate than the lower redshift ones. Nevertheless the total star formation rate for these galaxies is greater at $z = 4$ than at $z = 5.8$ because of the largest galaxies that have no counterpart at the earlier redshift. Since galaxies are observed only to limiting magnitudes, the mass evolution of galaxies by itself helps to explain why the luminosity function appears to evolve most at the bright end (Bouwens et al. 2006).

The star formation rates shown in Fig. 2 are measured in the simulations as the amount of stellar mass added in the previous 5 Myr. We have verified that, at $z = 6$, if that time interval is extended up to 60 Myr, the results barely change. Thus, galaxies in the simulations have extended periods of star formation. This point is important because it suggests that the observed luminous UV galaxies which have been used to estimate the total stellar density are a representative sample of all star-forming galaxies at $z \sim 6$ (Stark et al. 2006; Yan et al. 2006).

3.2. Effects of Numerical Resolution

Comparisons of apples and oranges are rarely useful, so in order to compare luminosities of simulated and observed galaxies, we need to know whether observations count all the light emitted from individual resolved galaxies, or if a substantial fraction of light remains undetected below the sky surface brightness. If the former, then a comparison between the simulations and the data is straightforward since it is easy to count all the emitted light in the simulations.

If, however, a substantial fraction of the light is not detected in the observations, the comparison with the simulations becomes much more difficult. In this case a simulation is required not only to get the total luminosity of the galaxy right, but also to correctly model the full spatial distribution of this luminosity as well.² The latter presents a much more serious challenge to modern simulations.

Unfortunately, we really have no way of knowing how much light is missed in the observations. One possible way of approaching this problem could be by using sufficiently high resolution simulations to resolve star forming regions and recover the correct light profile. We, therefore, first need to discuss the issues of numerical resolution in our simulations, because in our simulations galaxies do hide a significant albeit not dominant fraction of their luminosity below the surface brightness limit of current observations. Thus, we need to understand whether this is merely a resolution effect, or a property real galaxies might have too.

Numerical resolution affects simulated galaxies in diverse and complicated ways. Typically, simulations have constant spatial resolution in comoving units, with the real space physical resolution deteriorating with time. This effect would make later galaxies less concentrated than earlier ones. For our simulations, this effect is not tremendously large, since the difference between redshifts 4 and 5.8 is only about 40%. In addition, the cooling consistency condition implemented in the SLH

²One may argue that to get the total luminosity right, a simulation has to resolve the star forming regions as well. This is not the case, however, since all star formation prescription used in modern simulations incorporate free adjustable parameters, and one can phenomenologically fit the luminosity function of galaxies by properly adjusting parameters, without actually resolving the details of star formation.

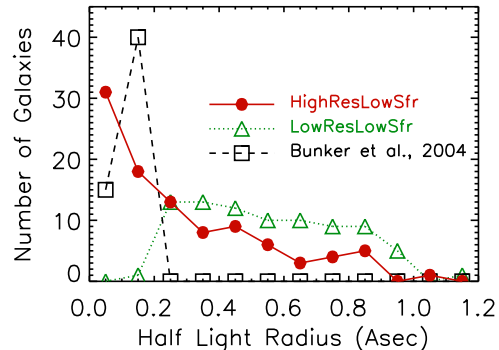


Fig. 3.— Distributions of half light radii of simulated galaxies brighter than $z_{850} = 29.5$ (unreddened) at $z \approx 6$ compared to observed galaxies (Bunker et al. 2004). For our cosmology 1 arcsec is 5.94 proper kpc.

code (Gnedin 1997) mitigates this effect further. Therefore, we might expect that if our spatial resolution is sufficient at $z = 5.8$, then it is also sufficient at $z = 4$.

However, one must also consider the mass resolution, whose effect usually goes in the opposite direction. As time in the simulation progresses, galaxies become more massive on average, i.e. they are represented by a larger number of resolution elements (dark matter and stellar particles, and gas cells). The number of resolution elements in a given galaxy, if not sufficient, would affect the sharpness of the central peak, which in turn could affect the spatial distribution of star formation. In our fiducial HighResLowSFR simulation a $10^{11} M_{\odot}$ halo consists of about 30,000 dark matter particles, a comparable number of baryonic cells, and about 10,000 stellar particles. Is this number sufficient to localize the star formation to within a few percent of the virial radius?³

Figure 3 attempts to address this question by showing the distribution of half light radii for simulated galaxies brighter than $z_{850} = 29.5$ (unreddened). The high resolution galaxies are more compact than the low resolution ones and, in some cases, as compact as the observed ones, but there

³For reference, the comoving virial radius of a $10^{11} M_{\odot}$ halo is about 100 comoving kpc, which translates into the angular diameter of $8''$ at $z = 4$ and $7''$ at $z = 5.8$.

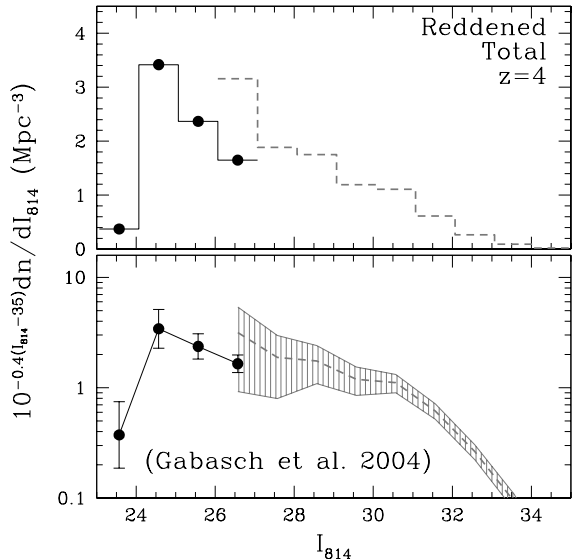


Fig. 4.— Total reddened luminosity functions at $z = 4$ for the LowResLowSFR simulation (dashed line) based upon galaxies larger than $10^{10} M_{\odot}$. The solid black line with error bars shows the observational data from Gabasch et al. (2004a). The top panel shows the linear scale along the y-axis, while the bottom panel shows the log scale. The hatched band around the LowResLowSFR simulation shows Poisson errors.

is still a substantial fraction (about 50%) of galaxies that are larger than the observed ones. Also, the significant difference between the LowResLowSFR and HighResLowSFR runs indicates that we have *not* reached the numerical convergence on the half light radii of simulated galaxies.

Therefore, in the rest of this paper, we will assume that our simulations do not properly resolve light profiles of most massive galaxies, and we will use the total luminosities of model galaxies.

3.3. Luminosity Functions of Model Galaxies

It is customary to present the luminosity function as a number density of galaxies per unit luminosity, dn/dL , or the number of galaxies per unit magnitude, dn/dm . In this paper we, however, are primarily concerned with estimating the star formation rate at various redshifts from luminosity functions, so the quantity of interest to us is the

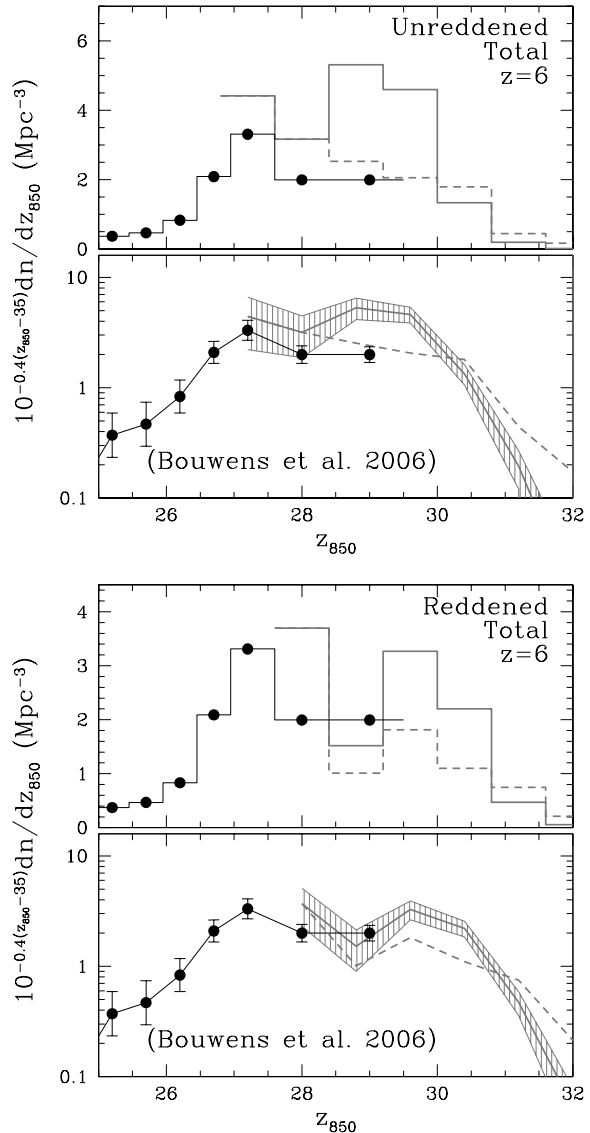


Fig. 5.— The same as in Fig. 4, but for $z = 5.8$, and showing in addition the HighResLowSFR run as the solid line within the hatched region. Two panels shows the unreddened and reddened luminosity functions respectively. The observational data are from Bouwens et al. (2006).

amount of light emitted per unit log in luminosity $L^2 dn/dL$, or, equivalently, per unit magnitude $10^{-0.4m} dn/dm$.

Figures 4 and 5 present the main result of this paper. The total (i.e. including all the light

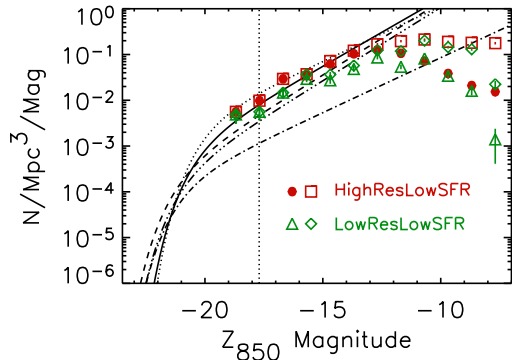


Fig. 6.— Comparison of faint ends of luminosity functions at $z = 6$. Shown are luminosity functions based upon the total galaxy population in the HighResLowSFR (red) and LowResLowSFR (green) simulations. Filled circles and triangles include all galaxies with total mass $M \gtrsim 1.28 \times 10^9 M_\odot$ (about 100 particles), and squares and diamonds all galaxies with total mass $M \gtrsim 3.84 \times 10^8 M_\odot$ (about 30 particles). Since the deepest observations extend only to the vertical dotted line, we have compared our results to the Schechter function fits to the observational data as presented in Table 12 of Bouwens et al. (2006). The line styles are long dash (Bouwens et al. 2006), dots (Dickinson et al. 2004), short dash (Yan & Windhorst 2004), dash dot (Bunker et al. 2004), and dash dot dot (Malhotra et al. 2005). The luminosity functions are independent of the mass cut off out to at least $z_{850} < -15$.

of model galaxies irrespective of surface brightness) luminosity functions from all our simulations are compared with the observational data from (Gabasch et al. 2004a) and (Bouwens et al. 2006). We show luminosity functions both with linear and log vertical scale, because the log plot allows one to see the whole range spanned by the values, while the linear scale is useful because the total luminosity (and, after an appropriate correction, the total star formation rate) is simply an area under the curve, which can be easily measured.

The overlap in magnitudes between the simulations and the observations is not large; simulations, because of their limited box size, are not able to produce the brightest, most rare galaxies. Observations, on the other hand, are missing the

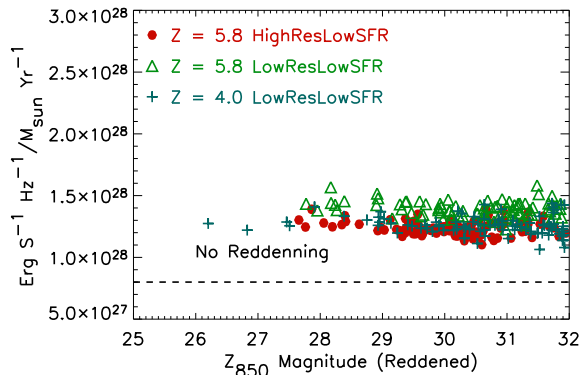


Fig. 7.— The ratio of star formation rate to the stellar luminosity at 1500 \AA (as measured by the z_{850} magnitude) as a function of magnitude for the simulated galaxies. The luminosities are calculated from the unreddened magnitudes and plotted as a function of reddened magnitudes. Shown are galaxies larger than $10^{10} M_\odot$. The dashed line shows the generally assumed value for this ratio (Madau et al. 1998).

majority of galaxies, that fall below the flux limit.

The advantage of using our choice for representing the galaxy luminosity function can now be illustrated. For example, it does appear that both the LowResLowSFR run and the observations are tracing the same luminosity function at $z = 4$. If we consider the combined curve as a true luminosity function, it can be estimated from the top panel of Fig. 4 that observations (without correcting for incompleteness) account for about 50% of the total star formation rate, while the simulation includes about 60% of the total SFR (with the overlap between the simulation and observations being 10% of the total).

The LowResHighSFR simulation (not shown) is a factor of 3 higher than the observational data, which is not surprising, since it has a 3 times higher star formation efficiency. Unless specifically noted, we use the LowSFR simulations for comparisons to the observational data.

The situation is different at $z = 5.8$. In the interval $27 \lesssim z_{850} \lesssim 29$, where the HighResLowSFR simulation overlaps with the observational data from Bouwens et al. (2006), the simulation predicts a factor of 2 more luminosity than

the data if no reddening correction is included, as argued by Stanway et al. (2005), which is about a 3σ deviation. With the reddening correction of Bouwens et al. (2006), the simulation agrees with the data (accounting for about 70% of the total luminosity, while the data also account for about 70% of the total light). The HighResLowSFR simulation is approximately consistent with the LowResLowSFR run, indicating that our simulated luminosity functions are close to the converged result (for the total luminosities of modeled galaxies).

We, thus, underscore the crucial importance of knowing the reddening corrections at $z \sim 6$ with sufficient precision. Studies of reddening agree that it is significantly less than at lower redshifts (see Bouwens et al. (2006) for summary).

A matter of considerable interest and debate is the slope of the faint end of the luminosity function when fitted to a Schechter function. Figure 6 compares our luminosity functions to various fits to observational data from the literature. The vertical line indicates the faintest level observed, which is achieved in the recent study by Bouwens et al. (2006). We refer the reader to this paper (Fig. 15 and accompanying discussion) for a comprehensive comparison of luminosity functions at $z \approx 6$ from the literature.

Simulation of the faint end of the luminosity function is limited by the minimum size galaxy that can be adequately resolved by the simulation. Since the exact number of dark matter and gas particles needed is uncertain, we show results for lower cutoffs of 100 and 30 particles for the LowResLowSFR simulation. To meaningfully compare the HighResLowSFR run we use the corresponding mass cutoffs (these will have 8 times as many particles). The results are the same out to $z_{850} < -13$. We find that, in contrast to the large galaxies of the previous figures, the smaller galaxies tend to be considerably less efficient at star formation. For this reason, we think it unlikely that a simulation with greater mass resolution would change the faint end slope in the region brighter than $z_{850} < -15$, fainter than can be currently observed.

To convert from luminosity to star formation rate, it is usually assumed that a luminosity at 1500 Å of 8×10^{27} erg/s/Hz corresponds to 1 solar mass of newly formed stars per year (Madau et al.

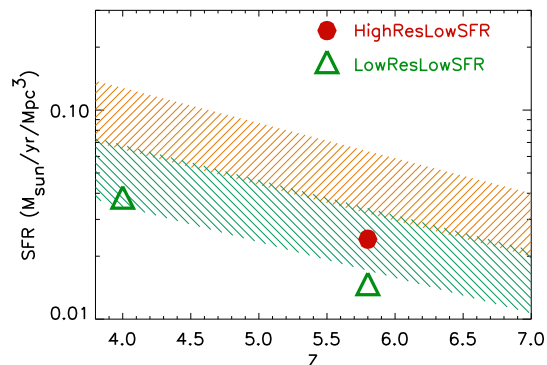


Fig. 8.— The star formation history in simulated galaxies brighter than 29.5 magnitude corrected for the finite size of the simulation box. The upper orange, hatched band shows the estimated range from Bouwens et al. (2006) using the conventional conversion factor (Madau et al. 1996). To facilitate comparison with the simulated galaxies, which show a different conversion factor, the upper band has been transposed down by a factor of 1.5 (lower green band) as explained in the text.

1998). This value, of course, depends upon the assumptions one uses for the population synthesis. We have used the more current “canonical” initial mass function given in Weidner & Kroupa (2006). In addition, we use a metallicity of $Z = 0.001$ (1/50th solar), which agrees better with the simulation than does the usual solar metallicity assumption (most of the simulated galaxies have metallicities well below 10% solar.). Figure 7 shows that our conversion factors are about 1.5 times higher than the conventional one. Of course, we do not know the true initial mass function and metallicity at these high redshifts. We emphasize the difference here to facilitate comparison of our results with the literature.

Figure 8, which summarizes our findings, is based upon a similar figure from Bouwens et al. (2006). The values are given to a limiting magnitude of 29.5. The upper hatched region shows the original range computed using the conventional conversion factor of 8×10^{27} erg/s/Hz per $1M_{\odot}/\text{yr}$. To facilitate comparison with our results, we also show this region transposed downwards by a factor of 1.5 to form the lower hatched region, to correspond to the conversion factor of

1.2×10^{28} erg/s/Hz per $1M_{\odot}/\text{yr}$ from Fig. 7. The star formation rates from our two LowSFR simulations *with the same magnitude cut* are also shown as individual symbols at $z = 4$ and $z = 5.8$. Both estimates agree with the data, although our value is slightly lower at $z = 4$ than the Bouwens et al. (2006) estimate. The small discrepancy is due to the fact that Bouwens et al. (2006) estimate is based on the Steidel et al. (1999) measurement, while our simulations agree best with Gabasch et al. (2004a), who find a somewhat lower value of star formation rate at $z \sim 4$. Gabasch et al. (2004b) considers their results to be in accord with those of Steidel et al. (1999).

3.4. Total Accumulated Stellar Mass Density

Recently infrared observations have enabled estimates of the accumulated stellar mass of high redshift galaxies. These results place constraints on prior generations of stars during the epoch of reionization and are an important test of cosmological simulations. Much of the observational data involves galaxies too rare to be present in the simulation box. Even so, the trends in the data are interesting.

Figure 9 shows a power law relation, which is nearly linear, between the star formation rate and the total stellar mass content of simulated galaxies at redshifts 4 and 5.8. These results agree broadly both in slope and magnitude with the hydrodynamic simulations of others (Night et al. 2006; Springel & Hernquist 2003; Finlator et al. 2006). In addition, their data extends beyond our highest points to about $10^{11} M_{\odot}$. At redshift 4 (top panel) the small overlap with the data of Feulner et al. (2005) is encouraging because the trends are similar. The solid line showing good agreement with the trend seen by Finlator et al. (2006) is noteworthy because of the very different techniques used in their simulations. The semi-analytic model in Idzi et al. (2004), by contrast, has considerably more scatter at this redshift. The spectroscopically verified galaxies of Stark et al. (2006) (bottom panel) exhibit a large spread, in contrast to the tight relationship in the simulated galaxies.

Contrasting observational results at a redshift of about 6 have been found by Yan et al. (2006). They find a population of galaxies with very high stellar masses but low star formation rates. These

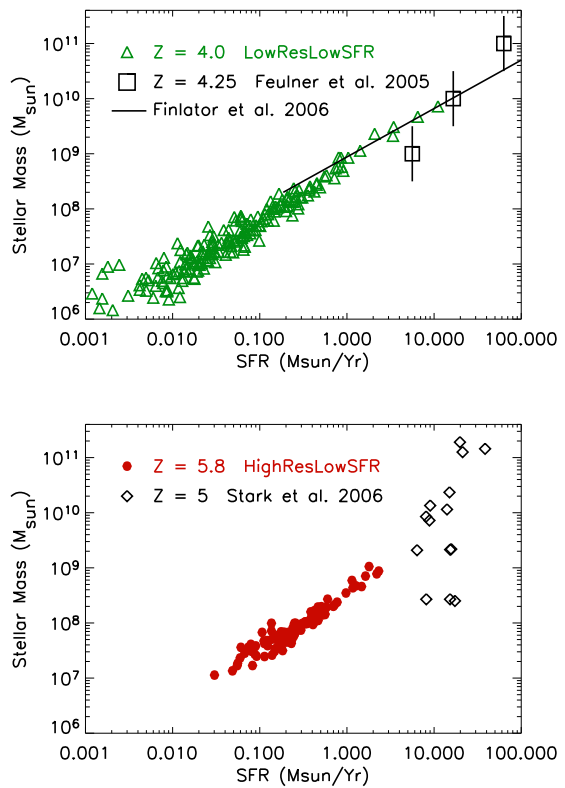


Fig. 9.— Stellar mass as a function of the star formation rate at $z = 4$ (top panel) and $z = 5.8$ (bottom panel) in the observations and the simulations (as labeled on the plots). Simulated galaxies shown are those larger than $10^{10} M_{\odot}$.

galaxies must have had higher rates of star formation in the past since the current star formation rate is insufficient to have formed the estimated stellar mass in the time since the Big Bang. We do not see any counterpart to this population. However, these galaxies are presumably very large and thus formed from density fluctuations too rare to be found in our simulation box; the effective volume of the Yan et al. (2006) observations is about 600 times larger than the volume of our simulation box.

The observational conversion from magnitude at 3.6 microns to stellar mass depends upon the unknown star formation histories of the galaxies. Since we know the star formation history of the simulated galaxies, it is useful to compute directly the expected observations. Fig. 10 shows

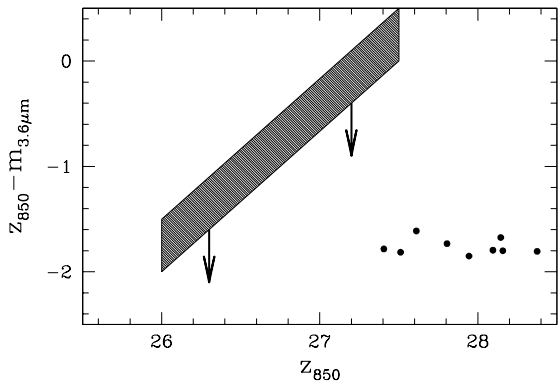
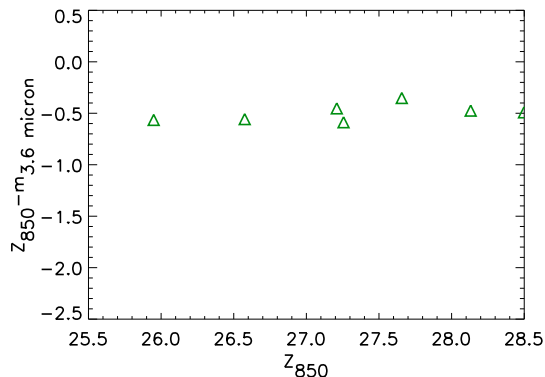


Fig. 10.— The $(z_{850} - m_{3.6\mu})$ colors vs magnitudes in the z_{850} passband for the simulated galaxies at $z = 4.0$ (top panel) and $z = 5.8$ (bottom panel). The shaded band in the bottom panel shows the upper limits for the 79 IRAC invisible galaxies from Yan et al. (2006).

$z_{850} - m_{3.6\mu}$) colors vs magnitude in the z_{850} passband for our two redshifts. There is little comparable observational data. We show in the bottom panel the IRAC invisible population of Yan et al. (2006) (Fig. 10, bottom panel). These are galaxies, which, although detectable in the rest frame UV, have too little stellar mass to be detected in the optical (infrared at this redshift). Little can be said except that these limits are at least consistent with our simulation results.

The star formation histories of the simulated galaxies larger than $10^{10} M_{\odot}$ at $z = 5.8$ are remarkably uniform. Figure 11 shows the average shape of this history to be a monotonically increasing function. Some individual galaxies show a decline

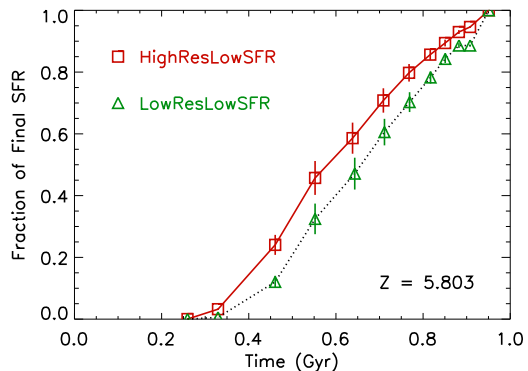


Fig. 11.— The average star formation rate profile for simulated galaxies at $z = 5.8$ with total mass larger than $10^{10} M_{\odot}$ as a function of time after the Big Bang. The error bars show the standard deviation.

of star formation rate typically beginning at 0.8–1.0 Gyr.

Figure 12 shows the history of the total stellar mass density of the simulations. Note that the LowResHighSFR simulation accumulates about three times as much mass, as one would expect from the 3 times greater star formation efficiency. It is difficult to compare these results to observations since these latter estimates are based on magnitude limited surveys. Nevertheless, these results reinforce our decision to use the lower star formation efficiency. The large arrow, showing the estimated stellar mass density at $z = 0$ (Cole et al. 2000), provides a ceiling, which should not be crossed.

4. Conclusions and Discussion

Despite its pivotal role in the evolution of the early universe, reionization remains poorly understood. As has been previously argued (Gnedin 2000), simulations provide important dynamical information inherently missing from analytic and semi-analytic approaches. This work is part of a continuing comparison of detailed cosmological simulations of reionization with observational data as they become available.

We have shown that numerical simulations of reionization that reproduce the SDSS data on the evolution of Gunn-Peterson absorption in spectra

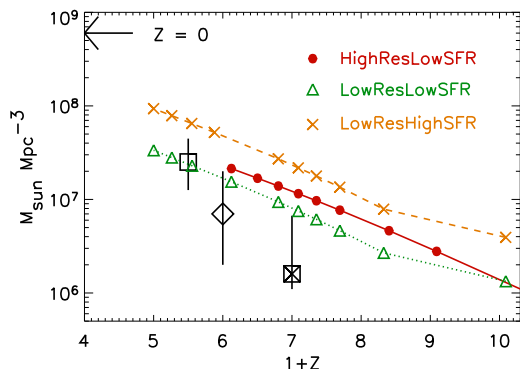


Fig. 12.— The evolution of the total stellar mass density in our three simulations (lines with symbols). The square, diamond, and square with X show observational results of (Drory et al. 2005), (Stark et al. 2006), and (Yan et al. 2006) respectively. Also shown for reference is the present day value from Cole et al. (2000) (arrow in upper left corner).

of $z \sim 6$ quasars can also be made consistent with the observed galaxy luminosity functions at two different redshifts ($z \sim 4$ and $z \sim 6$) *simultaneously* by adjusting a single parameter: a coefficient in the Schmidt law for star formation. The best-fit value of the coefficient is consistent with the observational estimates from local galaxies (Khokhlov 1998). In the best-fit case, the star formation rates per unit galaxy mass are similar to those found by Springel & Hernquist (2003) in their simulations using a very different numerical approach.

The simulations and much of the analysis for this paper were completed before the third year WMAP results (Spergel 2006) became available. The major change for structure formation is a lowering of σ_8 . The expected result is a delay in star formation, but the exact effect, of course, is not clear without new simulations. We have emphasized that the relative star formation rates at different redshifts are more amenable to analysis than are the absolute ones. Our single adjustable parameter would probably have to be modified for the new cosmology. Alvarez et al. (2006) has estimated the effect of the cosmological parameter changes on the collapsed fraction over a range of redshifts. The ratio of this fraction at $z \sim 4$ to that at $z \sim 6$ changes by a factor of about 1.5

between the two cosmologies. The expected direction of the effect would tend to bring the simulation into better agreement with observation (see Figure 8). It should be noted that the other hydrodynamic simulations to which we have compared our results have all used the higher value of σ_8 .

We are able to obtain agreement with the observed galaxy luminosity function at $z \sim 6$ if we consider all of the luminosity gravitationally bound to the galaxy and adopt the reddening correction of Bouwens et al. (2006). In addition, the total stellar mass densities at $z \approx 5$ to 6 are consistent with the latest observational estimates with the exceptions noted above.

Our results suggest that Lyman Break galaxies observed at $z \approx 6$ are the brightest ones at that time, with the caveat that the finite simulation box size limits the size of galaxies that we can simulate.

The simulation argues that the amount of star formation we see is sufficient to reproduce the reionization history imprinted on the Lyman- α forest.

The luminosity function of the simulation at $z = 5.8$ has been compared to the observational results of Bouwens et al. (2006) because their data overlap the simulation the most in magnitude. There seems to be general agreement that 28.5 is the limiting magnitude at which completeness becomes an issue. Another group (Bunker et al. 2004) has taken the conservative approach of confining the analysis to this limit. They have argued for a lower star formation rate with the consequence that other reionization sources, in addition to stars, might be necessary. Our results are not easily reconciled with these estimates, even when the uncertainty in the free parameters in the simulation, ie. the star formation efficiency and the effective escape fraction, are taken into account.

Le Fèvre et al. (2005) have made an exhaustive study of all galaxies seen to a limiting magnitude where the redshifts are determined spectroscopically. They argue that a significant fraction of galaxies out to redshift 5 is missed by Lyman Break selection techniques and that these missed galaxies significantly affect the ionizing photon budget. Their magnitude limit is much too low for these galaxies to be seen in our simulations. However, if these conclusions are found to extend

to higher redshifts the simulations will have to be modified to get a realistic picture of reionization. Larger box sizes, which at present are prohibitively expensive, may be necessary. For the present paper it is important to note that their results do support the notion that stars are sufficient for reionization.

All of our conclusions are limited by the size of the simulation box. The overall trend seen by Yan et al. (2006), in which the the largest galaxies have seen their zenith in the past, occurs over a much larger range of galaxy size than we can simulate. Over smaller ranges there is no clear trend, and thus our results are not inconsistent with existing data. However, we might have expected to see at least some trend in the simulation and we do not. As discussed by Finlator et al. (2006), the proportionality between star formation rate and stellar mass seen in hydrodynamic simulations may be an important limitation of these models. The semi-analytic model of Idzi et al. (2004), although it rests upon more assumptions, does at least produce more variability. Simulations with a much higher dynamic range may be needed to fully account for the population of galaxies contributing to reionization.

Even if it turns out that other reionization sources, not included in our simulations, are necessary, the correspondence of the simulated galaxies to observations of this period is of considerable interest since the simulation appears at least to reproduce the ionization state of the universe between redshifts 4 and 6.

The authors wish to thank the anonymous referee for helpful comments that improved the paper. This work was supported in part by the DOE and the NASA grant NAG 5-10842 at Fermilab, by the NSF grants AST-0134373 and AST-0507596, and by the National Computational Science Alliance grant AST-020018N, and utilized IBM P690 arrays at the National Center for Supercomputing Applications (NCSA) and the San Diego Supercomputer Center (SDSC). This work was begun while AGH was an associate member of the Center for Astrophysics and Space Astronomy at the University of Colorado at Boulder and completed at JILA. We wish to thank both institutes and A. J. S. Hamilton of JILA for support.

REFERENCES

- Alvarez, M. A., Shapiro, P. R., Ahn, K., & Iliev, I. T. 2006, *ApJ*, 644, L101
- Bertschinger, E. & Gelb, J. M. 1991, *Computers in Physics*, 5, 164
- Bouwens, R. J., Illingworth, G. D., Blakeslee, J. P., & Franx, M. 2006, *astro-ph*, 0509641, in press
- Bouwens, R. J., Illingworth, G. D., Thompson, R. I., Blakeslee, J. P., Dickinson, M. E., Broadhurst, T. J., Eisenstein, D. J., Fan, X., Franx, M., Meurer, G., & van Dokkum, P. 2004, *ApJ*, 606, L25
- Bunker, A. J., Stanway, E. R., Ellis, R. S., & McMahon, R. G. 2004, *MNRAS*, 355, 374
- Calzetti, D. 1997, *AJ*, 113, 162
- Cole, S., Lacey, C. G., Baugh, C. M., & Frenk, C. S. 2000, *MNRAS*, 319, 168
- Dickinson, M., Stern, D., Giavalisco, M., Ferguson, H. C., Tsvetanov, Z., Chornock, R., Cristiani, S., Dawson, S., Dey, A., Filippenko, A. V., Moustakas, L. A., Nonino, M., Papovich, C., Ravindranath, S., Riess, A., Rosati, P., Spinrad, H., & Vanzella, E. 2004, *ApJ*, 600, L99
- Drory, N., Salvato, M., Gabasch, A., Bender, R., Hopp, U., Feulner, G., & Pannella, M. 2005, *ApJ*, 619, L131
- Fan, X., Strauss, M. A., Becker, R. H., White, R. L., Gunn, J. E., Knapp, G. R., Richards, G. T., Schneider, D. P., Brinkmann, J., & Fukugita, M. 2006, *AJ*, in press
- Feulner, G., Gabasch, A., Salvato, M., Drory, N., Hopp, U., & Bender, R. 2005, *ApJ*, 633, L9
- Finlator, K., Davé, R., Papovich, C., & Hernquist, L. 2006, *ApJ*, 639, 672
- Gabasch, A., Bender, R., Seitz, S., Hopp, U., Saglia, R. P., Feulner, G., Snigula, J., Drory, N., Appenzeller, I., Heidt, J., Mehlert, D., Noll, S., Böhm, A., Jäger, K., Ziegler, B., & Fricke, K. J. 2004a, *A&A*, 421, 41

- Gabasch, A., Salvato, M., Saglia, R. P., Bender, R., Hopp, U., Seitz, S., Feulner, G., Pannella, M., Drory, N., Schirmer, M., & Erben, T. 2004b, *ApJ*, 616, L83
- Giavalisco, M., Dickinson, M., Ferguson, H. C., Ravindranath, S., Kretchmer, C., Moustakas, L. A., Madau, P., Fall, S. M., Gardner, J. P., Livio, M., Papovich, C., Renzini, A., Spinrad, H., Stern, D., & Riess, A. 2004, *ApJ*, 600, L103
- Gnedin, N. Y. 1997, *MNRAS*, 289, 927
- . 2000, *ApJ*, 535, 530
- . 2004, *ApJ*, 610, 9
- Gnedin, N. Y. & Abel, T. 2001, *New Astronomy*, 6, 437
- Gnedin, N. Y. & Fan, X. 2006, *ApJ*, 648, 1
- Harford, A. G. & Gnedin, N. Y. 2003, *ApJ*, 597, 74
- Hu, E. M., Cowie, L. L., Capak, P., & Kakazu, Y. 2005, in *IAU Colloq. 199: Probing Galaxies through Quasar Absorption Lines*, ed. P. Williams, C.-G. Shu, & B. Menard, 363–368
- Idzi, R., Somerville, R., Papovich, C., Ferguson, H. C., Giavalisco, M., Kretchmer, C., & Lotz, J. 2004, *ApJ*, 600, L115
- Khokhlov, A. M. 1998, *JCPH*, 143, 519
- Le Fèvre, O., Paltani, S., Arnouts, S., Charlot, S., Foucaud, S., Ilbert, O., McCracken, H. J., Zamorani, G., Bottini, D., Garilli, B., Le Brun, V., Maccagni, D., Picat, J. P., Scaramella, R., Scodreggio, M., Tresse, L., Vettolani, G., Zanichelli, A., Adami, C., Bardelli, S., Bolzonella, M., Cappi, A., Ciliegi, P., Contini, T., Franzetti, P., Gavignaud, I., Guzzo, L., Iovino, A., Marano, B., Marinoni, C., Mazure, A., Meneux, B., Merighi, R., Pellò, R., Pollo, A., Pozzetti, L., Radovich, M., Zucca, E., Arnaboldi, M., Bondi, M., Bongiorno, A., Busarello, G., Gregorini, L., Lamareille, F., Mathez, G., Mellier, Y., Merluzzi, P., Ripepi, V., & Rizzo, D. 2005, *Nature*, 437, 519
- Leitherer, C., Schaerer, D., Goldader, J. D., Delgado, R. M. G., Robert, C., Kune, D. F., de Mello, D. F., Devost, D., & Heckman, T. M. 1999, *ApJS*, 123, 3
- Madau, P., Ferguson, H. C., Dickinson, M. E., Giavalisco, M., Steidel, C. C., & Fruchter, A. 1996, *MNRAS*, 283, 1388
- Madau, P., Haardt, F., & Rees, M. J. 1999, *ApJ*, 514, 648
- Madau, P., Pozzetti, L., & Dickinson, M. 1998, *ApJ*, 498, 106
- Malhotra, S., Rhoads, J. E., Pirzkal, N., Haiman, Z., Xu, C., Daddi, E., Yan, H., Bergeron, L. E., Wang, J., Ferguson, H. C., Gronwall, C., Koekemoer, A., Kuemmel, M., Moustakas, L. A., Panagia, N., Pasquali, A., Stiavelli, M., Walsh, J., Windhorst, R. A., & di Serego Alighieri, S. 2005, *ApJ*, 626, 666
- Night, C., Nagamine, K., Springel, V., & Hernquist, L. 2006, *MNRAS*, 366, 705
- Oke, J. B. & Gunn, J. E. 1983, *ApJ*, 266, 713
- Shapley, A. E., Steidel, C. C., Adelberger, K. L., Dickinson, M., Giavalisco, M., & Pettini, M. 2001, *ApJ*, 562, 95
- Songaila, A. 2004, *AJ*, 127, 2598
- Spergel, D. N., Verde, L., Peiris, H., & et al. 2003, *ApJS*, 148, 175
- Spergel, D. N. e. a. 2006, *ApJ*, submitted
- Springel, V. & Hernquist, L. 2003, *MNRAS*, 339, 312
- Stanway, E. R., McMahon, R. G., & Bunker, A. J. 2005, *MNRAS*, 359, 1184
- Stark, D. P., Bunker, A. J., Ellis, R. S., Eyles, L. P., & Lacy, M. 2006, *astro-ph*, 0604250
- Steidel, C. C., Adelberger, K. L., Giavalisco, M., Dickinson, M., & Pettini, M. 1999, *ApJ*, 519, 1
- Weidner, C. & Kroupa, P. 2006, *MNRAS*, 365, 1333
- White, R. L., Becker, R. H., Fan, X., & Strauss, M. A. 2003, *AJ*, 126, 1
- Yan, H., Dickinson, M., Giavalisco, M., Stern, D., Eisenhardt, P. R. M., & Ferguson, H. C. 2006, *ApJ*, 651, 24
- Yan, H. & Windhorst, R. A. 2004, *ApJ*, 612, L93

